Journal of Umm Al-Qura University for Applied Sciences (2024) 10:491–509
https://doi.org/10.1007/s43994-023-00120-y

ORIGINAL ARTICLE

Activated *Opuntia ficus-indica* as an efficient adsorbent for iodine and heavy metals Cr(III), Cu(II) and Ni(II) ions uptake for wastewater treatment

Ahmed A. Alzharani[1]

Received: 30 September 2023 / Accepted: 23 December 2023 / Published online: 9 February 2024
© The Author(s) 2024

Abstract
Water pollution by heavy metals or iodine is a serious environmental issue that poses a threat to human health and ecosystems. Therefore, there is a need for developing efficient and low-cost methods for removing heavy metals and iodine from water sources. Activated *Opuntia ficus-indica* (AOFI) has been used for various purposes such as food, medicine, cosmetics, biofuel, and soil stabilization. The aim of this study was to investigate the feasibility of using AOFI as an adsorbent for removing heavy metals; e.g. Cr(III), Pb(II), and Cu(II) and iodine from water. The leaves of AOFI that were collected from Al-Baha city, KSA, were carbonized and characterized using FTIR spectroscopy and TGA analysis. Then uptake experiments were performed to evaluate the effects of various parameters such as pH, contact time, initial concentration, and temperature on the removal uptake by AOFI. Also the thermodynamic and kinetic parameters of the adsorption process had been calculated. The adsorption capacity of AOFI and OFI against iodine, Cr(III), Pb(II), and Cu(II) had been calculated. The results showed that; AOFI has adsorption capacity 1.14, 1.14, and 1.16 times higher than OFI, for Cr(III), Pb(II), and Cu(II), respectively, and 1.05 times higher than OFI, for iodine uptake. The findings indicated that AOFI exhibited remarkable efficacy in the metal ions uptake, achieving uptake efficiency up to 70%. Additionally, AOFI demonstrated notable efficiency in iodine uptake, reaching up to 60%. These results underscore the high uptake efficiency of AOFI for both metal ions and iodine, emphasizing its potential as an effective adsorbent for water treatment applications. This study is novel because it is the first to report the adsorption of heavy metals; such as Cr(III), Pb(II), and Cu(II) and iodine by AOFI.

Keywords Activated *Opuntia ficus-indica* (AOFI) · Heavy metal · Iodine · Kinetics

1 Introduction

Water pollution is one of the most serious environmental problems that threatens the health and well-being of humans and ecosystems [1–3]. Among the various pollutants, heavy metals and radioactive elements are of particular concern due to their toxicity, persistence, bioaccumulation and biomagnification [4]. Heavy metals such as chromium (Cr), copper (Cu) and nickel (Ni) are widely used in various industrial processes and can contaminate water sources through effluents, leaching and runoff [5]. Iodine is an essential element for human health, but excessive intake can cause thyroid disorders and other adverse effects [5]. Iodine can also be released into the environment from nuclear power plants, medical facilities and natural sources [1]. Therefore, it is necessary to develop effective and sustainable methods for the removal of these pollutants from water.

Among the various methods available for water treatment, adsorption is considered as one of the most promising techniques due to its simplicity, low cost, high efficiency and selectivity [2, 3]. Adsorption is the process of accumulation of solute molecules on the surface of a solid material, which is called the adsorbent. The adsorbent can be either natural or synthetic, and can have different physical and chemical properties that affect its adsorption capacity and affinity [5, 6]. The selection of an appropriate adsorbent is crucial for the success of the adsorption process [7, 8].

Opuntia ficus-indica (OFI) is a cactus that belongs to the Cactaceae family and originates from Mexico [9]. It is also known as cactus pear, prickly pear or barshumy in Arabic.

✉ Ahmed A. Alzharani
aas.alzahrani@bu.edu.sa

[1] Department of Chemistry, Faculty of Science, Al-Baha University, 65799 Al Baha, Saudi Arabia

OFI is a versatile plant that can grow in various climatic conditions and soil types, especially in arid and semi-arid regions [10]. It has high water-use efficiency and can tolerate drought, salinity and high temperatures. OFI produces edible fruits and cladodes (stem segments) that have nutritional, medicinal and industrial value [11]. OFI is widely cultivated in the Kingdom of Saudi Arabia, where it covers about 25,000 hectares of land, mainly in the Al Baha and Assir regions [12]. OFI is considered as a valuable resource for sustainable development in Saudi Arabia, as it can provide food, feed, fodder, biofuel, cosmetics, pharmaceuticals and other products. OFI can also enhance the food security and livelihoods of the rural population, especially in the dry areas, where it can cope with the effects of climate change and desertification. Moreover, OFI can conserve the natural resources and biodiversity of Saudi Arabia, by reducing the pressure on the scarce water and land resources and by restoring the degraded ecosystems. OFI has various applications in food, medicine, cosmetics and biofuel industries. It is also known for its high water storage capacity, which makes it resistant to drought and salinity [13, 14]. The main parts of OFI are the cladodes (stem segments) and the fruits, which contain high amounts of water, polysaccharides, phenolic compounds, vitamins, minerals and antioxidants [15]. These components can provide various functional groups, such as hydroxyl, carboxyl, amine and sulfhydryl, which can interact with metal ions and organic molecules [5].

One of the common methods of activation is the use of alkali agents, such as sodium hydroxide (NaOH), which can react with the organic components of the material and create pores and functional groups [5, 6, 16]. NaOH-activated OFI (AOFI) has been shown to have higher adsorption capacity and efficiency than raw OFI for the removal of various pollutants, such as dyes, phenols, nitrates and heavy metals. However, to the best of our knowledge, there is no study on the use of AOFI as an adsorbent for the removal of iodine and heavy metals Cr(III), Cu(II) and Ni(II) from water.

Thus these materials have emerged as efficient adsorbents for the removal of various pollutants from water, including heavy metals such as Cr(III), Pb(II), and Cu(II), as well as iodine [17–21]. The unique properties of these materials, such as their high surface area, tunable surface chemistry, and reactivity, make them effective in adsorbing and immobilizing these contaminants. The adsorption process involves the binding of heavy metal ions or iodine molecules onto the surface of materials through various interactions, such as electrostatic attraction, ion exchange, and complexation. Additionally, the porous structure of materials provides ample space for the accommodation of these contaminants. The application in water remediation not only offers high adsorption efficiency but also presents opportunities for sustainable and eco-friendly approaches to tackle water pollution. By exploring the potential of activated *Opuntia ficus-indica* as adsorbent, researchers aim to develop cost-effective and environmentally friendly solutions for the removal of heavy metals and iodine, contributing to the broader field of water purification and environmental protection.

2 The difference between activated *Opuntia ficus-indica* (AOFI) and other cactus

Activated *Opuntia ficus-indica* (AOFI) and unactivated *Opuntia ficus-indica* (OFI) are both types of cactus that can be used as biosorbents for the removal of metal ions or iodine from water [10, 22]. However, there are some differences between them in terms of their adsorption capacity, mechanism, and nutritional value. AOFI is treated by chemical or thermal methods to increase its surface functional groups and porosity, which can enhance its binding ability to metal ions and organic molecules [23, 24]. OFI is used in its raw form without any modification, relying on its natural mucilage content to adsorb metal ions through electrostatic and hydrogen bonding interactions [1]. AOFI has a higher adsorption capacity and kinetics than OFI for most metals, such as Ni, Pb, Cu, and Cd [23, 24]. However, OFI can also achieve a high removal efficiency of over 80% for these metals under optimal conditions [1]. AOFI and OFI have different effects on the iodine uptake and ascorbic acid content of the plant. AOFI can increase the ascorbic acid content and modify the vascular tissue in the plant when treated with iodine [25]. Therefore, AOFI can be a potential source of iodine for human consumption, as well as a green and efficient biosorbent for environmental remediation.

3 The superiorities of activated *Opuntia ficus-indica* (AOFI) over the other materials

Activated *Opuntia ficus-indica* (AOFI) can be used as a renewable and eco-friendly adsorbent for the removal of organic and inorganic pollutants from water, such as dyes, heavy metals, and iodine [26–28]. AOFI has some superiorities over other materials in the metal uptake or iodine uptake [29]. AOFI is abundant, cheap, and easy to obtain, unlike some synthetic or commercial adsorbents that are expensive, scarce, or require complex preparation methods [10]. AOFI has a high surface area, porosity, and reactivity, which enhance its adsorption capacity and efficiency [5]. AOFI can be activated by treating it with an alkaline solution, such as sodium hydroxide, which increases its surface area, porosity, and reactivity even more. AOFI has a rich content of functional groups, such as hydroxyl, carboxyl, and amine groups, which can form complexes or bonds with the pollutants. AOFI can also adsorb pollutants through physical

mechanisms, such as electrostatic attraction, van der Waals forces, or hydrogen bonding. AOFI can adsorb a wide range of pollutants, such as malachite green dye, Cu(II), Ni(II), and iodine, with high removal efficiencies and uptake capacities [25]. AOFI can adsorb pollutants at different pH values, temperatures, and contact times, showing its versatility and adaptability. AOFI can also adsorb pollutants in both single- and multi-component systems, showing its selectivity and compatibility. Therefore, AOFI is a promising material for the metal uptake or iodine uptake, as it has many advantages over other materials in terms of availability, cost, performance, and applicability.

Therefore, the aim of this study was to investigate the potential of OFI and AOFI as an efficient adsorbent for the removal of iodine and heavy metals Cr(III), Cu(II) and Ni(II) from aqueous solutions. The effects of various parameters, such as pH, contact time, initial concentration and temperature, on the adsorption process were studied. The adsorption kinetics, isotherms and thermodynamics were also analyzed to understand the mechanism and nature of the adsorption process. The results of this study can provide valuable information for the development of a novel and eco-friendly adsorbent for water treatment.

4 Methodology

4.1 Materials

The *Opuntia ficus-indica* (OFI) was collected from Al-Baha city area in Saudi Arabia. The metal salts; $Cr(NO_3)_3 \cdot 9H_2O$, $Pb(NO_3)_2$, and $Cu(NO_3)_2 \cdot 3H_2O$, and iodine were purchased from Sigma-Aldrich. Nitric acid (65%) and NaOH were analytic grade. All solutions were prepared with de-ionized water. Atomic absorption spectroscopy (AAS) was used for quantification of metal ion concentration in solutions.

4.2 Preparation

The Al-Baha city region in Saudi Arabia is the source for the cactus. The dust and other surface contaminants on the cactus were cleaned up using distilled water, which was used to wash the plant. After being hacked up into smaller bits, the *Opuntia ficus-indica* (OFI) was allowed to dry at room temperature. The OFI was dehydrated first, then crushed, and then sieved for later usage. After that, the OFI was activated by impregnating them with NaOH using weight ratios of 1:1 between the OFI and the NaOH, as was documented in the relevant literature [30]. The technique consisted of dissolving 17 g of NaOH in 300 mL of distilled water, and then adding 17 g of OFI to achieve a ratio of 1:1 between the OFI and NaOH. After that, the solution was agitated constantly for two hours, and then it was dried in an oven at 100 °C with hot air until all of the moisture was eliminated. As a consequence of this, the impregnated dry OFI was carbonized at a temperature of 500 °C for one hour. The product that was developed after activation was given the designation of "Activated *Opuntia ficus-indica*" (AOFI). To get rid of ash as well as acid-soluble contaminants, the product was washed again in hot distilled water with 0.1 M HCl, and then again in distilled water until the pH was about 7. After that, the materials were heated to 100 °C to remove moisture from them until they were totally dry. The energized *Opuntia ficus-indica* was put away for possible usage in the future.

The stock solution of metal ions was prepared in water with concentration of 100 ppm, and then diluted to 50 ppm. Furthermore, the stock iodine solution was prepared in hexane with concentration of 100 ppm, and then diluted to 50 ppm (Fig. 1).

4.3 Characterization

The OFI, and AOFI were characterized using FT-IR, thermal gravimetric analysis (TGA), and powder-XRD.

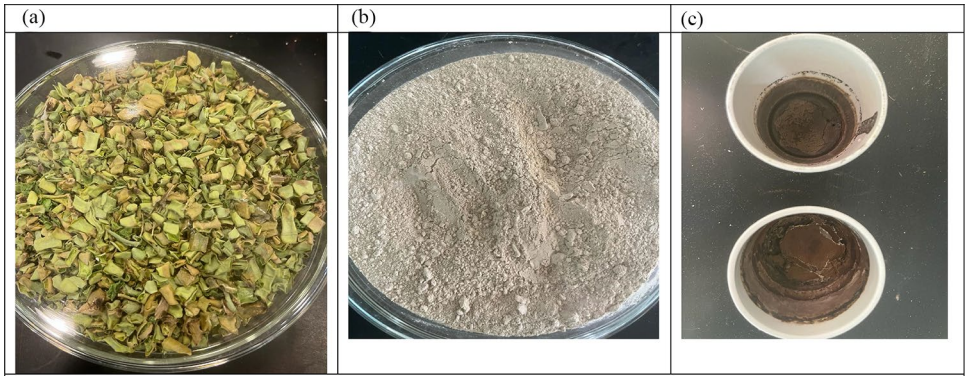

Fig. 1 Showing the **a** *Opuntia ficus-indica* (OFI) cutting pieces. **b** *Opuntia ficus-indica* (OFI) after drying and grounded process. **c** Activated *Opuntia ficus-indica* AOFI

4.4 Uptake tests

4.4.1 General protocol

The metal ion/iodine uptake tests were carried out by combining a definite volume of a metal ion/iodine solution of solution of known initial concentration (50 ppm) as shown in Table 1, with a definite volume of the OFI, or AOFI. A magnetic stirrer was used to stir the solution at a constant speed and a predetermined pH (the pH was brought to the correct level using either HNO_3 or NaOH solution). All of these procedures were carried out at a constant 25 °C. In the case of metal ion uptake, the metal ion solution had been collected and filtered after certain amount of time had passed. AAS was then used to quantify the amounts of metal ions in the resultant solution after acidification with HNO_3 (6 mL) and HCl (2 mL). In the case of iodine uptake, the absorbance of the filtered supernatant was evaluated at 525 nm via UV–Vis spectroscopy after an established period of time had passed.

4.4.2 Effect of pH

The batch approach was used to establish the optimum pH for maximum metal ion/iodine uptake by the OFI, or AOFI

Table 1 Batch tests experimental conditions of metal ion/iodine uptake

Parameter	Solution pH	OFI/AOFI (g/L)		Contact time (min)		Metal ion/iodine volume (mL)	Total volume (mL)
		Metal ion	Iodine	Metal ion	Iodine		
Solution pH	1.88	0.55	0.70	150	240	5.00	10.00
	2.68						
	4.13						
	5.08						
	5.86						
	7.11						
	8.67						
	9.78						
OFI/AOFI (g/L)	7.11	0.10		150	240	5.00	10.00
		0.25					
		0.40					
		0.55					
		0.70					
		0.85					
		1.00					
		1.15					
Contact time (min)	7.11	0.55	0.70	15		5.00	10.00
				30			
				60			
				90			
				150			
				240			
				360			
				480			
Metal ion/iodine initial concentration	7.11	0.55	0.70	150	240	1.00	10.00
						2.00	
						3.00	
						4.00	
						5.00	
						6.00	
						7.00	
						8.00	

Initial concentration of metal ion/iodine = 50 ppm, at temperature of 25 °C, and stirring rate of 500 rpm. The final optimum conditions were; ttemperature = 25 °C, stirring rate = 500 rpm, pH = 7.11, OFI/AOFI concentration = 0.55 g/L (for metal ion uptake) and 0.70 mg/L (for iodine uptake), contact time = 150 min (for metal ion uptake) and 240 min (for iodine uptake), metal ion/iodine concentration = 25 ppm

at 0.55 g/L (in the case of metal ion uptake) or 0.70 g/L (in the case of iodine uptake). OFI, or AOFI was combined with 5.0 mL of a metal ion/iodine solution of known initial concentration (50 ppm), as shown in Table (1). A magnetic stirrer was used to agitate the liquid at a constant rate of 500 rpm for 150 min while the pH was changed as; 1.88, 2.68, 4.13, 5.08, 5.86, 7.11, 8.67, and 9.78, as shown in Table 1. After each experiment, the final solution's metal ion/iodine concentration had been calculated using AAS, and by absorbance evaluation at 525 nm, respectively. The metal ion/iodine uptake percentage (%) had been calculated using Eq. (1). Where; the initial concentration and final concentration were denoted by $C_{initial}$, and C_{final}, respectively.

$$\% \text{ Removal} = ((C_{initial} - C_{final}) \times 100)/C_{initial} \quad (1)$$

4.4.3 Effect of OFI, or AOFI initial concentration

Adsorbent mass impact on heavy metal ion/iodine uptake was determined by using the batch technique with varying quantities of the tested materials. A metal ion/iodine solution (5.0 mL) with a known initial concentration (50 ppm) was combined with OFI, or AOFI at concentrations of 0.10, 0.25, 0.40, 0.55, 0.70, 0.85, 1.00, and 1.15 g/L. Table 1 show the conditions of 150 min (for metal ion uptake) and 240 min (for iodine uptake) of swirling at 500 rpm with a magnetic stirrer at a constant pH of 7.11. After each experiment, the final solution's metal ion/iodine concentration had been calculated using AAS, and by absorbance evaluation at 525 nm, respectively. The percentage of metal ion/iodine uptake was calculated using Eq. (1).

4.4.4 Contact time and kinetics

Furthermore, the time required for uptake to achieve equilibrium was calculated. The batch procedure was used for this purpose. For metal ion/iodine uptake experiment, the OFI, or AOFI at 0.55 g/L (in the case of metal ion uptake) or 0.70 g/L (in the case of iodine uptake), and 5.0 mL of a metal ion/iodine solution with a known initial concentration (50 ppm) were included. At a constant pH (7.11), the mixture was swirled for varying contact time (15, 30, 60, 90, 150, 240, 360, and 480 min) using a magnetic stirrer, Table 1. After each experiment, the final solution's metal ion/iodine concentration had been calculated using AAS, and by absorbance evaluation at 525 nm, respectively. The percentage of metal ion/iodine uptake was calculated using Eq. (1).

Pseudo first order, Eq. (2), and pseudo second order, Eq. (3), were used at different contact times to assess the kinetic behavior, Tables 1.

$$Ln(Q_e - Q_t) = LnQ_e - K_1 t \quad (2)$$

$$\frac{t}{Q_t} = \frac{t}{Q_e} + \frac{1}{K_2 Q_e^2} \quad (3)$$

where, the K_1, K_2, and t are the pseudo-first order rate constant, the pseudo-second order rate constant, and the contact time. Q_t, Q_e, are defined as the time-dependent and equilibrium adsorption capacities, respectively.

4.4.5 Effect of metal ion/iodine initial concentrations and isotherm

Metal ion/iodine uptake was studied using the batch technique at varying metal ion/iodine initial concentrations to draw conclusions about this impact. The batch procedure was used for this purpose. OFI, or AOFI [0.55 g/L (in the case of metal ion uptake) or 0.70 g/L (in the case of iodine uptake)] were combined with metal ion/iodine solutions quantities of (1.00, 2.00, 3.00, 4.00, 5.00, 6.00, 7.00, and 8.00 mL) with an initial concentration of 50 ppm [31]. A magnetic stirrer was used to stir the mixture at a fixed rate of 500 revolutions per minute for a total of 150 min (in the case of metal ion uptake) and 240 min (in the case of iodine uptake) at a constant pH of 7.11, Table 1. After each experiment, the final solution's metal ion/iodine concentration had been calculated using AAS, and by absorbance evaluation at 525 nm, respectively. The metal ion/iodine uptake percentage was calculated using Eq. (1).

Both the Langmuir, Eq. (4), and the Fiendish, Eq. (5), isotherms were used to analyze the metal ion/iodine uptake behavior of solutions of the metal ion/iodine at different initial concentrations, Table 1.

$$\frac{1}{Q_e} = \left(\frac{1}{Q_m K_L}\right)\frac{1}{C_e} + \frac{1}{Q_m} \quad (4)$$

$$LnQ_e = LnK_f + \frac{1}{n}LnC_e \quad (5)$$

where C_e is the adsorbate equilibrium concentration in parts per million, Q_e is the equilibrium metal ion/iodine uptake capacity in milligrams per gramme of adsorbent, Q_m is the maximum monolayer coverage capacity in milligrams per gramme of adsorbent, K_L is the Langmuir constant in liters per milligram of adsorbent, and K_f is the Fiendish constant.

4.5 Recyclability and reusability of AOFI

After each adsorption cycle, carefully the AOFI adsorbent was collected. Implement a regeneration procedure to desorb or remove the adsorbed pollutants by washing with appropriate solvents, acid treatment. Then, the regenerated AOFI

was dried to remove any residual moisture. Then, repeating the adsorption process for five cycles, and measure the adsorption capacity of AOFI after each cycle to evaluate its performance over time.

5 Results and discussions

5.1 Characterization

5.1.1 FT-IR of OFI, and AOFI

The temperature dependence of the FT-IR spectra in oxygen-free conditions is seen in Fig. 2. When analyzing the OFI's organic components, FT-IR typically provides characteristics from organic functional groups. OFI's high intensity peak at 3448 cm^{-1} is consistent with organic O–H stretching, while water or another mineral containing a hydroxyl group may have contributed to its formation. The loss of hydrogen and oxygen atoms due to bond breakage from the hydroxyl group is reflected as a reduction in hydroxyl peak intensity after thermal treatment (in the case of AOFI).

5.1.2 Thermal analysis (TGA and DGA) of OFI, and AOFI

Figure 3 displays the thermal expansion and contraction curves of OFI, and AOFI. Burning OFI progressed through four distinct phases. Between 25 and 145 °C, mass loss occurred mostly as a result of evaporation of water, with the DTA peak occurring at 95 °C. Two DTA peaks, at 285 and 415 °C, indicate that devolatilization and OFI combustion followed [32]. At 630 °C, a DTA peak corresponding to the burning of carbon residue occurred. The quick release and burning of the OFI volatiles resulted in a net mass loss of 77.38%. The combustion profile of AOFI was quite different from that of OFI. The DTA curve of AOFI exhibited one peak at 465 °C, which corresponded to the mass loss (about 64.86%) resulting from devolatilization and subsequent burning of volatile substances and char. The peak of AOFI production clearly occurred after the OFI peak and was narrower.

5.1.3 XRD of OFI, and AOFI

XRD stands for X-ray diffraction, which is a technique that can reveal the structure and composition of materials by measuring how X-rays are scattered by the atoms in the sample. *Opuntia ficus-indica* (OFI) and Activated *Opuntia ficus-indica* (AOIF) are two types of cactus plants that have different XRD patterns. OFI and AOIF have different XRD patterns because they have different properties. OFI is mainly composed of cellulose, hemicellulose, lignin, pectin, and mucilage, which are biopolymers that form the cell wall and the extracellular matrix of the plant. AOIF is obtained by treating OFI with an alkaline solution, sodium hydroxide, which removes some of the hemicellulose and lignin, and modifies the structure and composition of the remaining biopolymers. The alkaline treatment also activates the surface of OFI, making it more porous and reactive. The different biopolymers and the degree of activation

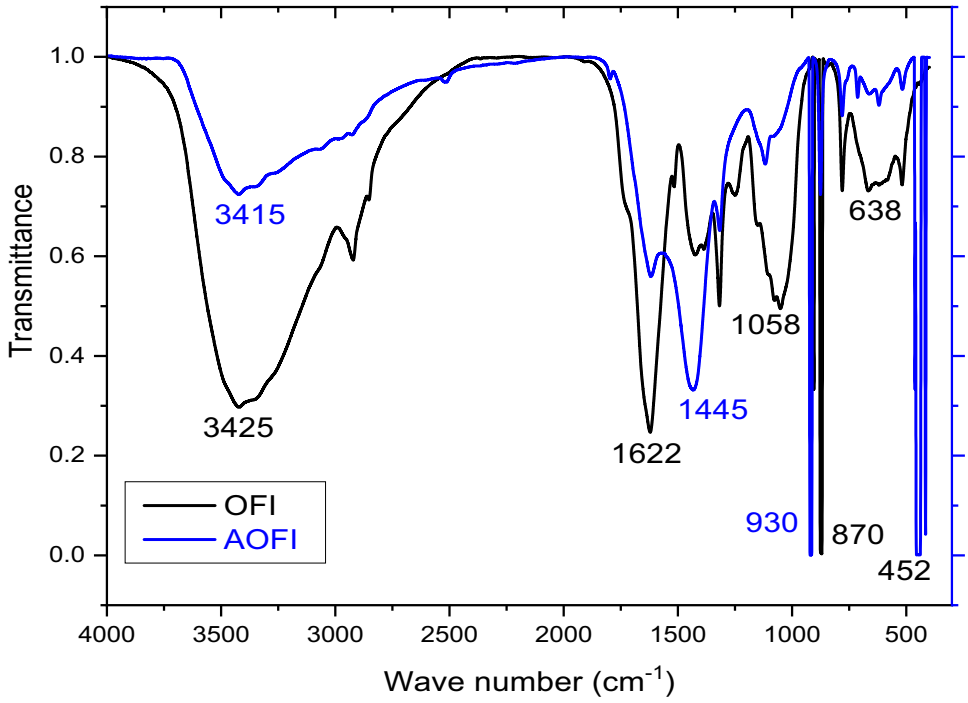

Fig. 2 FT-IR for OFI, and AOFI

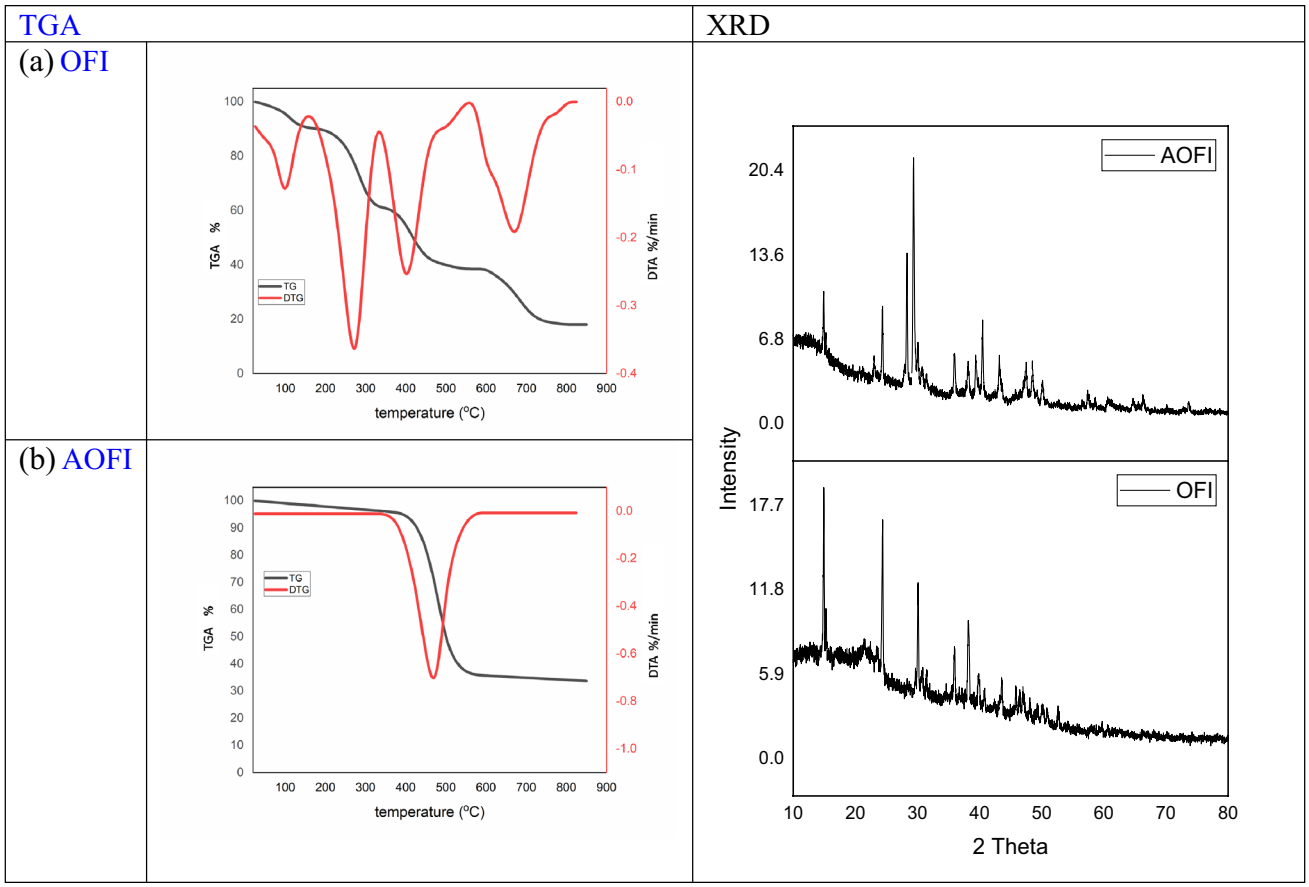

Fig. 3 TGA, DTA, and XRD curves of OFI, and AOFI

affect the XRD patterns of OFI and AOIF, as they change the crystallinity, the orientation, and the spacing of the atomic planes in the material. The XRD patterns of OFI and AOIF can be seen in Fig. 3. The XRD patterns of OFI show main peaks at $2\theta = 14.80°$, 24.46°, 29.95°, 35.76°, 38.32°. The XRD patterns of AOIF show a shift of the peaks to higher angles, indicating a decrease in the interplanar spacing and an increase in the crystallinity of the material. The XRD patterns of AOIF show main peaks at $2\theta = 15.13°$, 24.98°, 28.25°, 30.45°, 36.97°, 40.38°.

5.2 Metal ions uptake

5.2.1 pH effect

The pH value plays a crucial role in the uptake of metals, influencing the ionization of functional groups on the adsorbent surface and the chemical speciation of metal ions in the sorbate [33]. In this study, a series of batch tests was systematically conducted at different pH levels (1.88, 2.68, 4.13, 5.08, 5.86, 7.11, 8.67, and 9.78) to comprehensively assess the impact of pH on the uptake of Cr(III), Pb(II), and Cu(II). This experimental approach aimed to elucidate the intricate relationship between pH variations and the adsorption efficiency of the metals, providing valuable insights into the pH-dependent mechanisms governing the sorption process. Through meticulous examination across a range of pH conditions, the study sought to establish a comprehensive understanding of how variations in the solution's acidity or alkalinity influence the adsorption behavior of the investigated heavy metal ions.

Around neutral pH levels, approximately 7, as illustrated in Fig. 4, the adsorbents exhibit a remarkable capacity for the uptake of Cr(III), Pb(II), and Cu(II) ions, showcasing the highest percentage of removal. However, this efficiency experiences a sharp decline at both lower and higher pH values. At lower pH values, hydrogen ions competitively interact with metal ions for transferable cations on the sorbent surface, resulting in a notable reduction in sorption [34]. Interestingly, the metal uptake sites appear to exhibit increased sensitivity to pH changes between the pH range of 4 and 6, leading to a moderate upturn in metal uptake. Beyond a pH of 7, Cr(III), Pb(II), and Cu(II) ions tend to precipitate as hydroxides, contributing to a deceleration in the uptake rate and a reduction in the capacity for heavy metal removal. This phenomenon can be attributed to the

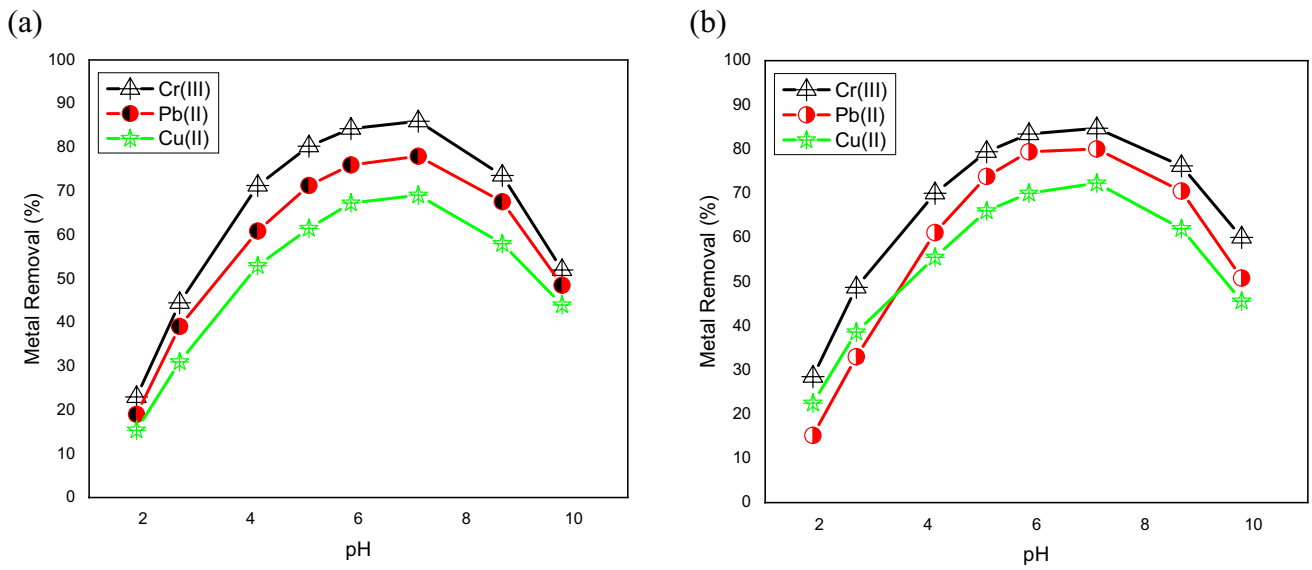

Fig. 4 pH change on the heavy metals uptake onto 0.55 g/L of the **a** OFI and **b** AOFI, with 150 min contact time, and T = 25 °C

elevated concentration of Na^+ in the solution, a consequence of pH adjustment using NaOH, displacing the remaining Cr(III), Pb(II), and Cu(II) ions from the exchangeable sites. This nuanced understanding sheds light on the intricate pH-dependent mechanisms influencing the adsorption behavior of the studied metal ions.

5.2.2 Adsorbent mass effect

The mass of the adsorbent emerges as a pivotal factor influencing the uptake capacity of metal ions. To scrutinize the influence of adsorbent quantity on the uptake of Cr(III), Pb(II), and Cu(II) by the investigated materials, batch tests were systematically conducted with varying samples ranging from 0.10, 0.25, 0.40, 0.55, 0.70, 0.85, 1.00, and 1.15 g/L. The findings, as depicted in Fig. 5, underscore the necessity for a higher quantity of adsorbent to achieve equivalent levels of heavy metal uptake across the studied materials. This phenomenon can be attributed to the persistent unsaturation of metal uptake sites throughout the adsorption process, commonly referred to as "active centers" [35]. Following impregnation, the surface area and pore volume

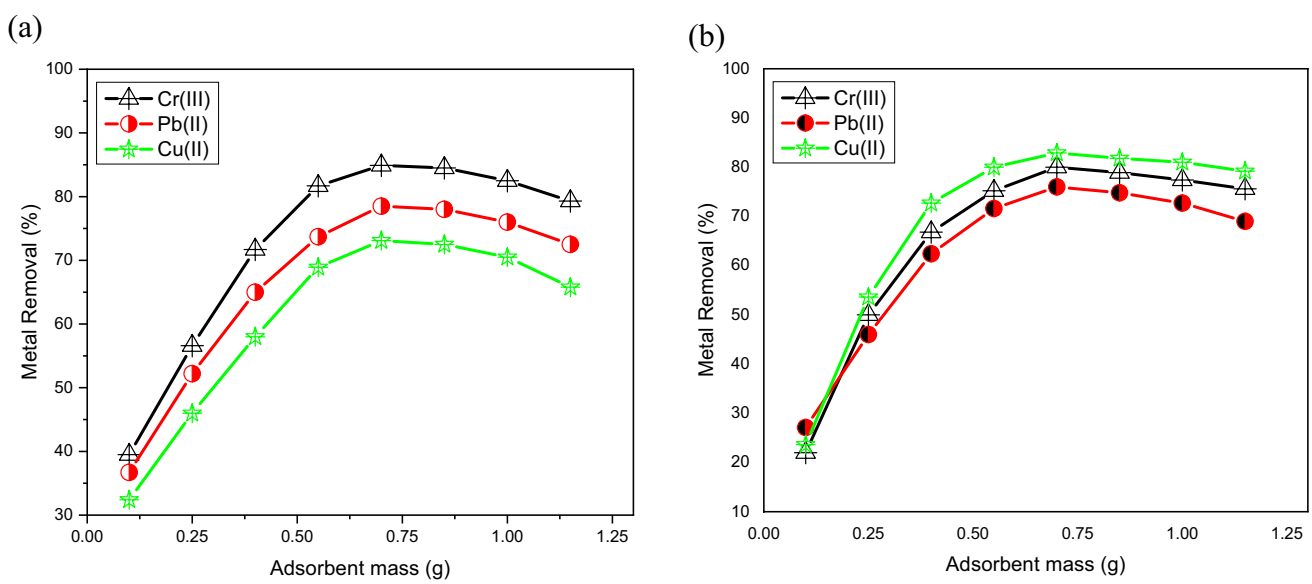

Fig. 5 Adsorbent mass effect on heavy metals adsorption onto the **a** OFI and **b** AOFI, with 150 min contact time, T = 25 °C and pH = 7.11

of the adsorbent experience augmentation, leading to an intensified concentration of these active sites. This substantiates the observed enhancement in performance with the addition of more adsorbent. The nuanced interplay between adsorbent mass and metal uptake efficiency offers valuable insights into optimizing conditions for enhanced heavy metal removal.

5.2.3 Kinetics and contact time effect

The temporal aspect of the sorption process, commonly known as contact time, is a critical determinant influencing its efficiency [36]. As depicted in Fig. 6, the impact of contact duration on the adsorption of Cr(III), Pb(II), and Cu(II) onto the investigated materials is elucidated. The findings unveil a rapid elimination of Cr(III), Pb(II), and Cu(II) ions that gradually diminishes over time until equilibrium is attained. Specifically, the initial 150 min of the sorbate-sorbent interaction witness a heightened sorption rate for all three metals, primarily attributed to the increased accessibility of the adsorbent's surface area during the initial stages of the process. Subsequently, as the adsorption sites become depleted, the removal rate becomes negligible. This two-stage sorption mechanism aligns with well-established literature [9, 36–38], wherein the first phase is characterized by rapid and substantial sorption, while the subsequent phase is more gradual and contributes relatively less to the overall process. Understanding these temporal dynamics is crucial for optimizing the efficiency of metal ion removal processes.

Through modifications to the pseudo-first order (Eq. 2) and pseudo-second order (Eq. 3) [39] kinetics models, the kinetics outcomes were derived. Figure 7 illustrates the values of the pseudo-first order rate constant (K_1), pseudo-second order rate constant (K_2), and the corresponding contact times (t). Additionally, the time-dependent adsorption capacities (Q_t) and equilibrium adsorption capacities (Q_e) were determined. These parameters provide insights into the temporal dynamics of the sorption process and help characterize the efficiency of the studied materials in removing Cr(III), Pb(II), and Cu(II) ions over varying contact times. The adjustments made to these kinetic models facilitate a more accurate representation of the sorption behavior, enabling a comprehensive understanding of the adsorption mechanisms at play during different stages of the process.

The obtained R^2 values, as depicted in Fig. 7, indicate that the pseudo-second-order kinetic model serves as the most suitable fit for describing the uptake kinetics of Cr(III), Pb(II), and Cu(II). These findings strongly suggest that the process of Cr(III), Pb(II), and Cu(II) uptake follows a chemisorption mechanism [40, 41]. This inference is drawn from the fact that Cr(III), Pb(II), and Cu(II) ions establish robust covalent bonds with the surfaces of the materials, implying a high level of chemical interaction. Notably, electron-donating functional groups, such as electron-rich hydroxyl groups [42, 43], play a pivotal role in enhancing the material's capacity to sequester Cr(III), Pb(II), and Cu(II). The chemisorptive nature of the process underscores the significance of surface interactions in dictating the kinetics of heavy metal uptake by the studied materials.

5.2.4 Initial concentration

The removal percentages of Cr(III), Pb(II), and Cu(II) ions, illustrated in Fig. 8, exhibit variability based on

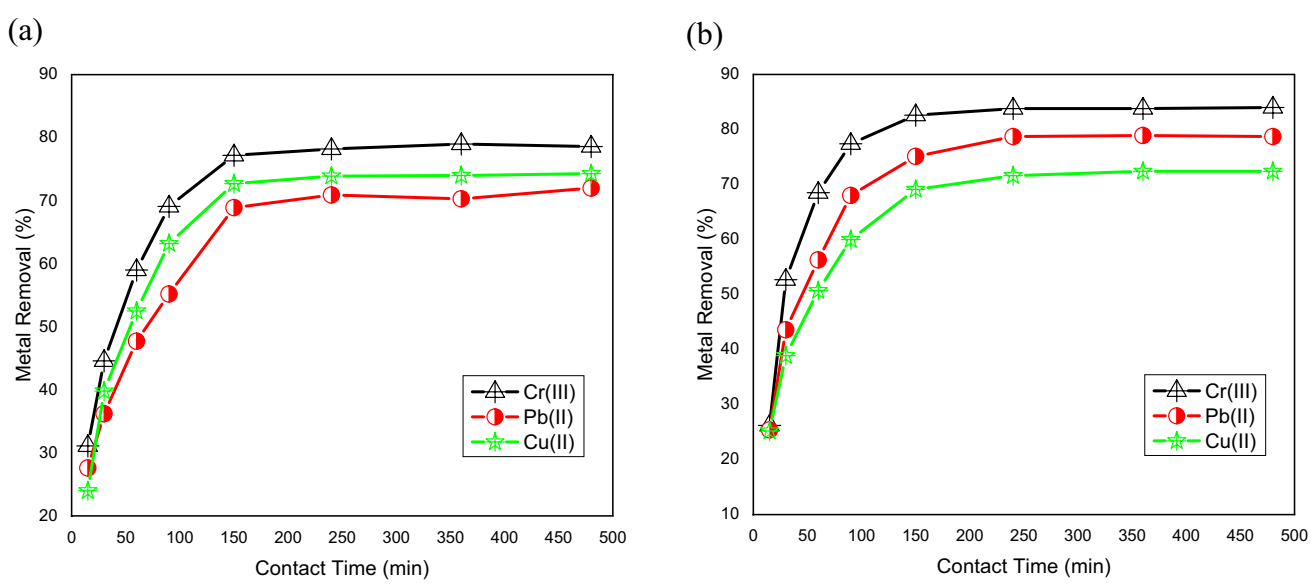

Fig. 6 Contact time effect of heavy metals adsorption onto the **a** OFI and **b** AOFI, at T = 25 °C and pH = 7.11

(a)

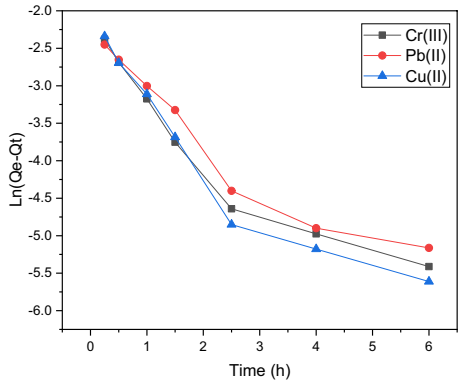

	Cr(III)	Pb(II)	Cu(II)
R^2	0.88357	0.90417	0.88227
K_1	0.52746	0.50221	0.57902

(b)

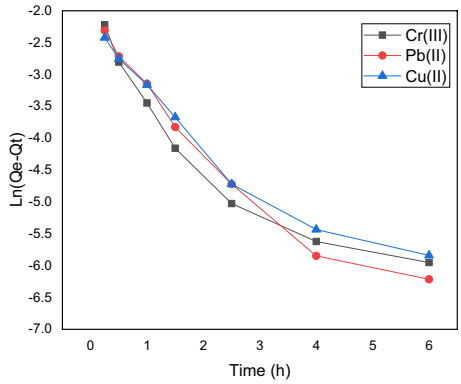

	Cr(III)	Pb(II)	Cu(II)
R^2	0.85987	0.93026	0.92237
K_1	0.63084	0.70321	0.61518

(c)

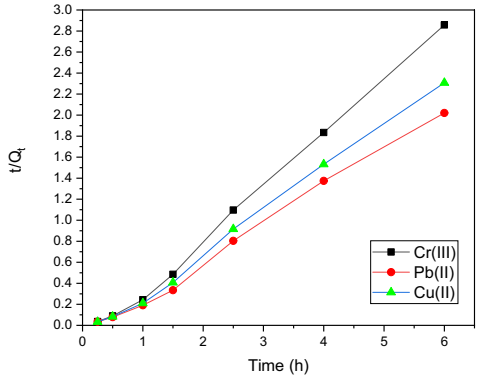

	Cr(III)	Pb(II)	Cu(II)
R^2	0.99826	0.99736	0.99825
K_2	0.50426	0.35965	0.4089

(d)

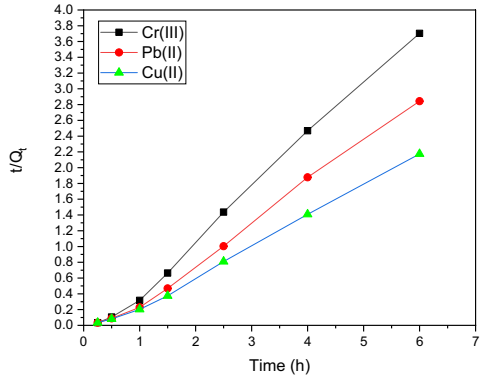

	Cr(III)	Pb(II)	Cu(II)
R^2	0.99845	0.99753	0.99838
K_2	0.66054	0.50582	0.38197

Fig. 7 Pseudo-first-order framework for **a** OFI and **b** AOFI; pseudo-second-order framework for **c** OFI and **b** AOFI

the initial metal concentration, ranging from 2.00 to 16.00 ppm. It is evident from the results that the removal efficiency of Cr(III), Pb(II), and Cu(II) ions is directly proportional to the initial concentration. As the concentrations of Cr(III), Pb(II), and Cu(II) exceed 5.67 ppm, starting at 8.18 ppm, 10.25 ppm, and reaching 15.38 ppm, both the removal efficiency and uptake rate experience a decline. This phenomenon can be attributed to the fact that, at higher initial concentrations, a limited number of sites on the adsorbent surface can effectively adsorb the ions, resulting in a high uptake site-to-initial-concentration ratio. Conversely, this ratio diminishes as the initial concentration of Cr(III), Pb(II), and Cu(II) increases, leading to the saturation of specific adsorption sites. Consequently, the percentage of removal becomes contingent on the concentration prior to removal [44].

The adsorption capacity had been calculated by using the Eq. (6) [45]. Where; C_i is the Initial concentration in ppm, C_e is the concentration at equilibrium, m is the mass of the adsorbent, V is the volume of solution containing solute (adsorbate). The adsorption capacities were estimated, Fig. 8. The results showed that; AOFI has adsorption capacity 1.14, 1.14, and 1.16 times higher than OFI, for Cr(III), Pb(II), and Cu(II), respectively.

(a)

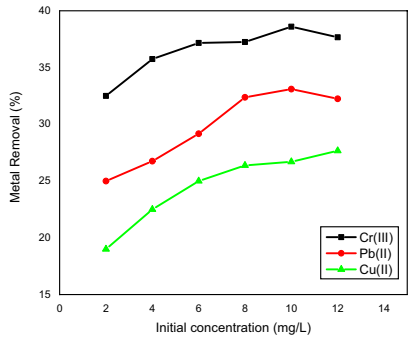

	Cr(III)	Pb(II)	Cu(II)
Adsorption Capacity	476.00	460.91	446.18

(b)

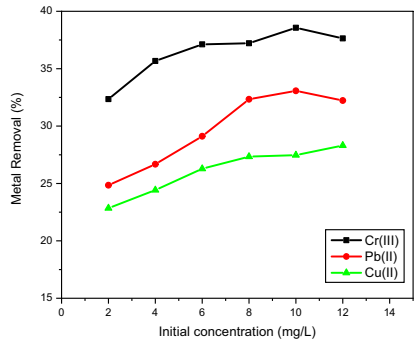

	Cr(III)	Pb(II)	Cu(II)
Adsorption Capacity	541.76	526.31	515.58

(c)

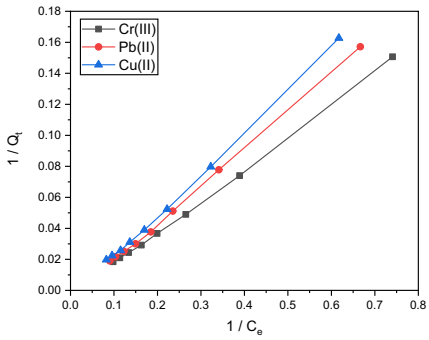

	Cr(III)	Pb(II)	Cu(II)
R^2	0.99921	0.99958	0.9994

(d)

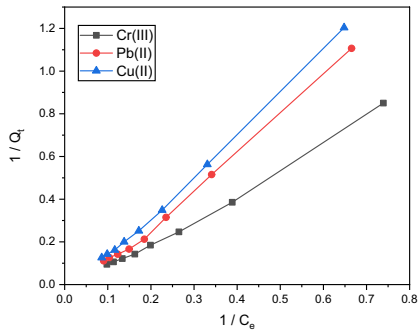

	Cr(III)	Pb(II)	Cu(II)
R^2	0.99697	0.99776	0.99887

(e)

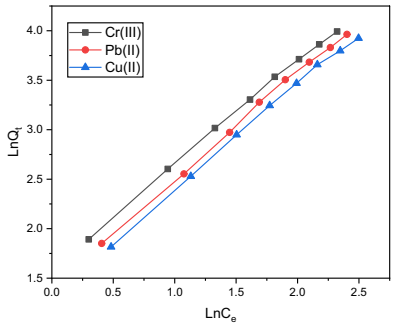

	Cr(III)	Pb(II)	Cu(II)
R^2	0.99935	0.9991	0.99894

(f)

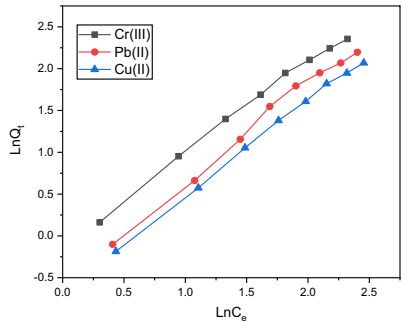

	Cr(III)	Pb(II)	Cu(II)
R^2	0.9974	0.99575	0.99896

Fig. 8 Initial concentration effect on the adsorption of Cr(III), and Pb(II), as well as Cu(II) onto the **a** OFI and **b** AOFI, Langmuir model of **c** OFI and **d** AOFI, and Freundlich model of **e** OFI and **f** AOFI. (At pH 7.11 and T = 25 °C)

$$\text{Adsorption Capacity (mg/g)} = \left[\left(C_i - C_e\right) \times V\right]/m \quad (6)$$

The utilization of uptake isotherms is crucial in elucidating the spatial distribution of the adsorbate within the liquid and the adsorbent. These isotherms hinge on assumptions related to the homogeneity or heterogeneity of adsorbents, the extent of coverage, and the existence of a potential relationship between the adsorbent and the adsorbate [38]. Various isotherm models are available to characterize the distribution of metal ions between the liquid and solid phases [46]. Notably, among these models, the Langmuir model and Freundlich's model stand out as effective tools in comprehending the complex interplay between adsorbents and adsorbates in different scenarios.

The foundational principle of the Langmuir model, represented by Eq. (4), is the adsorption of substances onto a surface in a monolayer, utilizing a finite number of receptors that share similar characteristics and an evenly distributed adsorption energy [47, 48]. According to this model, once a spot is fully saturated, there can be no additional sorption at that specific site. The linear correlation between ($1/Q_e$) and ($1/C_e$) depicted in Fig. 7 unequivocally indicates that the adsorption process adheres to the Langmuir model. This relationship emphasizes the restricted nature of adsorption sites and the uniformity of adsorption energy distribution across the surface.

The Freundlich isotherm equation (Eq. 5) [49] introduces adsorbate-specific parameter K_f, adsorbent-specific parameter n, and equilibrium concentration (C_e) in milligrams per milliliter. Through linear regression, the temperature-dependent constants K_f and 1/n can be determined. These constants, influenced by the Freundlich treatment, represent the binding energies between the metal ion and the adsorbent (parameter n) and the bond strength (parameter K_f). The parameter n offers insights into the likelihood of sorption occurrence, with favorable sorption qualities typically observed for n values between 2 and 10, challenging qualities for values between 1 and 2, and subpar qualities for values below 1 [50]. Figure 8 depicts the linearized Freundlich isotherms for Cr(III), Pb(II), and Cu(II), revealing that the studied materials exhibited somewhat favorable adsorption constants for these ions, with n values hovering around one. The calculated model parameters, along with the correlation coefficient (R^2) for various models, are illustrated in Fig. 8. In terms of model fit, the Langmuir model demonstrates a better agreement with the adsorption isotherm.

5.3 Iodine uptake

5.3.1 Adsorbent mass

The quantity of adsorbent mass plays a pivotal role in determining uptake capacity. Various quantities of OFI or AOFI (0.10, 0.25, 0.40, 0.55, 0.70, 0.85, 1.00, and 1.15 g/L) were employed in batch studies to assess the influence of adsorbent dosage on iodine uptake. The data, presented in Fig. 9, elucidates that an increase in the adsorbent amount correlates with a proportional enhancement in iodine uptake on the studied materials. This phenomenon can be attributed to the maintenance of unsaturated uptake sites throughout the process [35], commonly referred to as "active centers." Following impregnation, the adsorbent experiences an augmentation in surface area and pore volume, leading to a heightened concentration of these active sites. Consequently, the addition of more adsorbent manifests improved performance in iodine uptake.

5.3.2 Contact time and kinetics

The temporal aspect, specifically contact time, stands as a crucial factor influencing sorption dynamics [36]. The graphical representation in Fig. 10 elucidates the impact of contact time on the iodine uptake onto the studied materials. This observation unveils a pattern wherein the initial iodine uptake is rapid, followed by a subsequent decrease over time until a state of equilibrium is attained. Notably, the first 240 min of the sorbate-sorbent interaction witness a heightened rate of iodine uptake, attributed to a more extensive availability of adsorbent surface area for metal uptake. However, as the uptake sites become swiftly exhausted, the iodine uptake rate diminishes, ultimately reaching a negligible level. This two-stage uptake phenomenon aligns with established literature [9, 36–38], wherein the initial stage is characterized by rapid and substantial quantity-driven

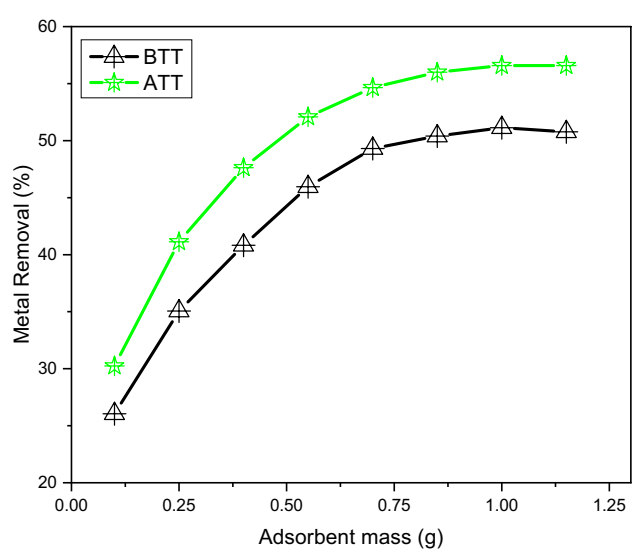

Fig. 9 Adsorbent mass change on the iodine uptake onto the OFI and AOFI, with contact time of 240 min, at T = 25 °C and pH = 7.11

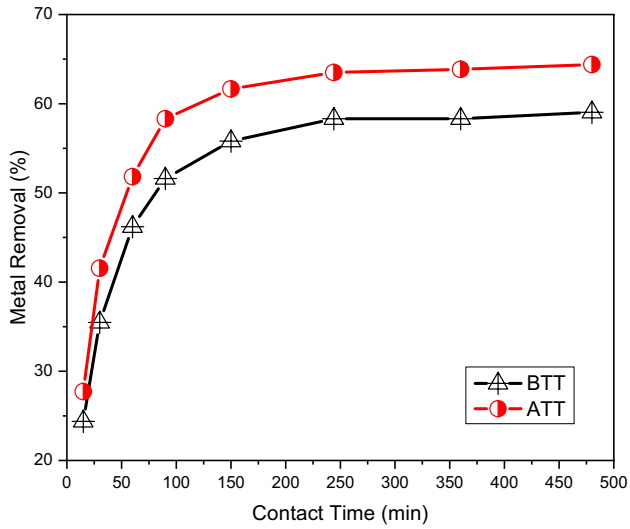

Fig. 10 Contact time of iodine uptake onto the OFI and AOFI, at T = 25 °C and pH = 7.11

uptake, while the subsequent stage is a more gradual and less impactful process.

The findings of the kinetics investigation were derived by modifying the pseudo first order Eq. (2) and pseudo second order Eq. (3) [39]. In these equations, Q_t represents the uptake capacity as a function of time (mg/g), Q_e denotes the uptake capacity at equilibrium (mg/g), K_1 signifies the pseudo-first order rate constant, K_2 corresponds to the pseudo-second order rate constant, and t symbolizes the contact time. The graphical representation in Fig. 11 visually depicts the correlation between these parameters, offering a comprehensive insight into the temporal dynamics of the adsorption process.

The obtained R^2 values depicted in Fig. 11 establish that the dynamics governing the uptake of iodine are most accurately described by the pseudo-second-order kinetic model. These outcomes strongly imply that the process of iodine absorption follows a chemisorption mechanism [40, 41], indicating a robust and stable bond formation between iodine and the adsorbent surfaces. The heightened affinity of iodine to surfaces is indicative of the chemisorptive nature of the interaction, emphasizing the strength and durability of the iodine adsorption process.

5.3.3 Initial concentration and equilibrium isotherm

In Fig. 12, the percentage of iodine uptake is illustrated across different initial iodine concentrations (5, 10, 15, 20, 25, 30, 35, and 40 ppm). The results demonstrate a consistent increase in the percentage of iodine uptake with rising initial concentrations until reaching a saturation point at 30 ppm. This observation emphasizes the direct correlation between the initial concentration of iodine and the corresponding proportion of iodine uptake, highlighting the influence of the starting conditions on the adsorption capacity [44].

The analysis of uptake isotherms serves as a fundamental tool in examining the spatial arrangement of the adsorbate within the liquid and the adsorbent, incorporating considerations of adsorbent heterogeneity/homogeneity, coverage characteristics, and the potential interaction between the adsorbent and adsorbate [38]. Multiple isotherm models, such as the Langmuir model and Freundlich's model, can be

(a)

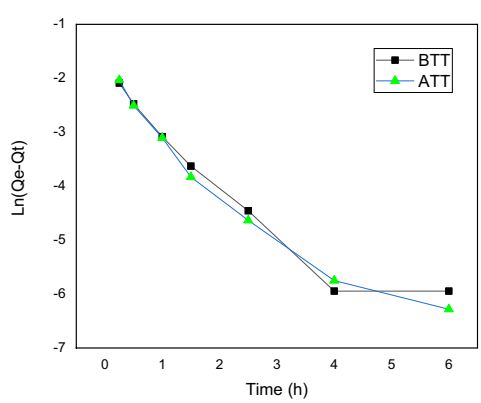

	OFI	AOFI
R^2	0.9024	0.9172

(b)

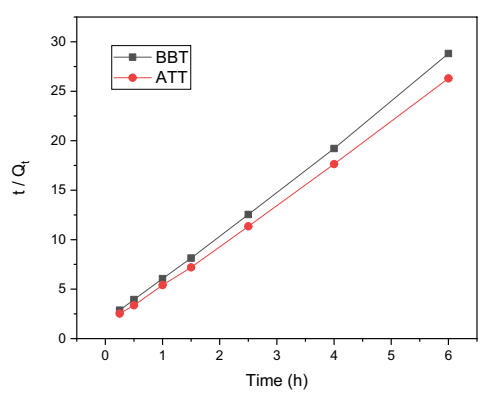

	OFI	AOFI
R^2	0.9992	0.9993

Fig. 11 **a** Pseudo-first-order model and **b** pseudo-second-order model for iodine uptake onto the investigated material OFI and AOFI, at T = 25 °C and pH = 7.11

(a)

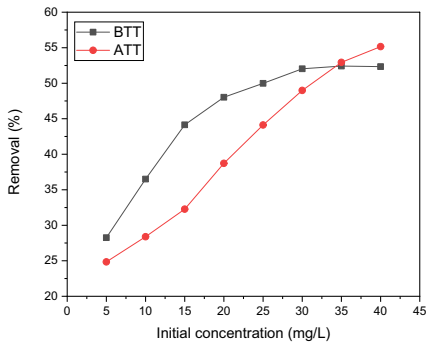

	OFI	AOFI
Adsorption Capacity	299.10	315.18

(b)

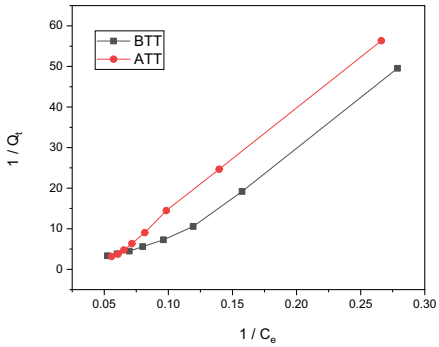

(c)

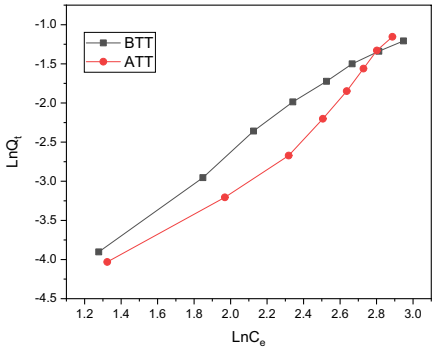

	OFI	AOFI		OFI	AOFI
R^2	0.98695	0.99964	R^2	0.9962	0.98256

Fig. 12 **a** Initial concentration change on the iodine uptake onto the investigated substance. **b** Langmuir model and **c** Freundlich model for iodine uptake over OFI and AOFI. (At pH 7.11 and T = 25 °C)

applied to elucidate the distribution of iodine between the liquid and solid phases [46]. The Langmuir model, expressed by Eq. (4), is based on the premise of monolayer adsorption, where substances adhere to a surface with a limited number of similar sites and uniform adsorption energy. Once a site is fully saturated, no further uptake occurs at that specific location [47, 48]. The observed linear relationship between ($1/Q_e$) and ($1/C_e$) in Fig. 12 attests to the Langmuir model's appropriateness for accurately describing the iodine uptake process.

The expression of the Freundlich isotherm is delineated by Eq. (5) [49], wherein K_f and n represent adsorbate and adsorbent-specific parameters, and C_e signifies the equilibrium concentration in milligrams per milliliter. Through the application of linear regression, the temperature-dependent constants K_f and 1/n can be ascertained. The Freundlich treatment unveils essential information about the binding energies between the metal ion and the adsorbent, with the parameter n reflecting the strength of the bond, and K_f representing the bond strength, both parameters determined by the Freundlich treatment. The n values derived from the Freundlich equation offer valuable insights into the likelihood of sorption occurrence. Generally, sorption is considered favorable within the range of n values between 2 and 10, while values between 1 and 2 present challenges, and those below 1 are deemed subpar [50]. In the plotted linearized Freundlich isotherms for iodine in Fig. 12, all the n values hover around one, indicating that the studied materials exhibit only moderate effectiveness in adsorbing iodine. Figure 12 also presents the predicted model parameters alongside the correlation coefficient (R^2). In terms of model fit, the Langmuir model emerges as a superior match to the adsorption isotherm.

The adsorption capacity had been calculated by using the Eq. (6) [45]. Where; C_i is the Initial concentration in ppm, C_e is the concentration at equilibrium, m is the mass of the adsorbent, V is the volume of solution containing solute (adsorbate). The adsorption capacities were estimated, Fig. 8. The results showed that; AOFI has adsorption capacity 1.05 times higher than OFI, for iodine uptake.

5.4 Limit of detection

Using the Eqs. (7, and 8), the limit of detection (LOD) and the limit of quantification (LOQ) are determined.

$$\text{LOD} = (3 \times \text{ standard deviation})/\text{slope} \quad (7)$$

$$\text{LOQ} = (10 \times \text{ standard deviation})/\text{slope}) \quad (8)$$

The relative standard deviation was determined by measuring the absorption of 8 samples. The calibration curve was obtained by varying the concentration of metal ions from 5.0 to 40.0 ppm, Fig. 13. To calculate the slope, a linear regression model was used for the calibration values. The LOD was determined to be 30.47, 32.99, and 29.65 ppm, for Cr(III), Pb(II), and Cu(II), respectively, in the case of using OFI. While the LOD was determined to be 20.91, 22.01, and 19.28 ppm, for Cr(III), Pb(II), and Cu(II), respectively, in the case of using AOFI. Furthermore, the LOD was determined to be 58.72, and 44.00 ppm, for iodine uptake, in the case of using OFI, and AOFI, respectively.

5.5 Recyclability and reusability of AOFI

The recyclability and reusability of AOFI are crucial aspects contributing to its sustainability as an adsorbent.

(a)

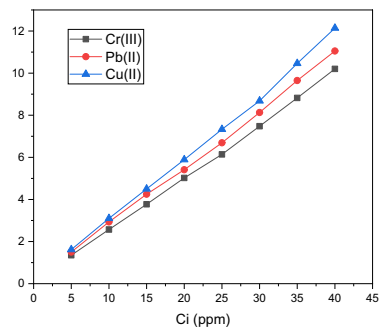

	Cr(III)	Pb(II)	Cu(II)
LOD	30.47	32.99	29.65
LOQ	118.37	118.40	118.43

(b)

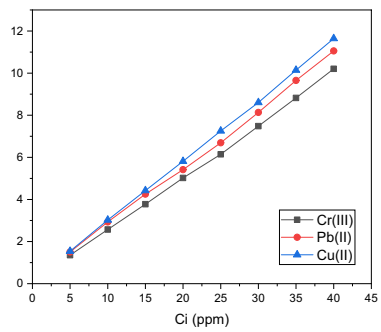

	Cr(III)	Pb(II)	Cu(II)
LOD	20.91	22.01	19.28
LOQ	118.37	118.40	118.33

(c)

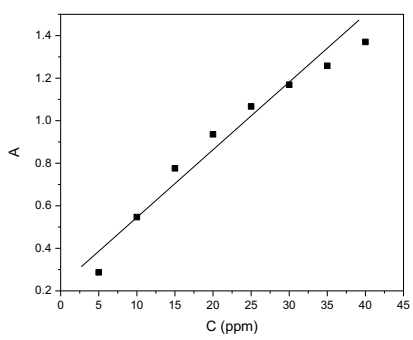

LOD	58.72
LOQ	120.79

(d)

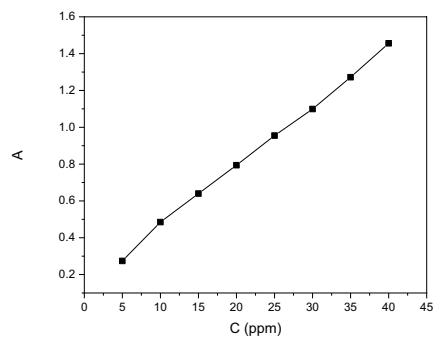

LOD	44.00
LOQ	118.42

Fig. 13 The calibration curve for Cr(III), Pb(II), and Cu(II) uptake, in the case of **a** OFI, and **b** AOFI, and the calibration curve for iodine uptake, in the case of **c** OFI, and **d** AOFI

In this study, AOFI exhibited good recyclability characteristics, showcasing its ability to be regenerated and reused multiple times without significant loss of adsorption capacity. After undergoing five cycles of regeneration, AOFI retained more than 80% of its initial adsorption capacity, indicating robust and consistent performance over successive applications.

The recyclability of AOFI is attributed to its inherent properties, such as its structural integrity and the preservation of active sites responsible for metal and iodine uptake. During regeneration, the activated material effectively maintained its adsorption efficiency, highlighting its resilience to the regeneration process.

This feature is particularly advantageous for practical applications, as it minimizes the need for frequent replacement of the adsorbent, reducing operational costs and environmental impact. The ability of AOFI to endure multiple cycles of use underscores its potential for sustainable water treatment practices.

Furthermore, the reusability of AOFI contributes to its economic viability and aligns with the principles of green and eco-friendly technologies. The robust recyclability of AOFI positions it as a promising candidate for long-term and cost-effective applications in water treatment, emphasizing its suitability for addressing environmental challenges associated with heavy metal and iodine pollution.

5.6 Metal ions/iodine uptake comparison

The adsorption capacity data for Cr(III), Pb(II), and Cu(II) uptake by both OFI and AOFI, as well as the adsorption capacity data for iodine uptake by AOFI, were evaluated and compared, revealing significant differences in performance. AOFI exhibited superior adsorption capabilities, with adsorption capacities 1.14, 1.14, and 1.16 times higher than OFI for Cr(III), Pb(II), and Cu(II), respectively. Moreover, AOFI demonstrated a 1.05 times higher adsorption capacity than OFI for iodine uptake. These results underscore the enhanced adsorption performance of AOFI across a range of heavy metal ions and iodine compared to its precursor, OFI. Additionally, the limit of detection (LOD) data further emphasized the improved sensitivity of AOFI. The LOD for Cr(III), Pb(II), and Cu(II) using AOFI was notably lower than that using OFI, with values of 20.91, 22.01, and 19.28 ppm, respectively, compared to 30.47, 32.99, and 29.65 ppm, respectively. Furthermore, the LOD for iodine uptake using AOFI (44.00 ppm) was considerably lower than that using OFI (58.72 ppm). These findings highlight the superior adsorption efficiency and enhanced detection sensitivity of AOFI, making it a promising material for effective removal of metal ions and iodine from aqueous solutions.

5.7 Comparison with previous literature survey

The adsorption capacity and limit of detection (LOD) of Cr(III), Pb(II), Cu(II), and iodine by AOFI were compared with those reported by other researchers in previous studies. The maximum adsorption capacities of AOFI for Cr(III), Pb(II), Cu(II), and iodine, which were 541.76, 526.31, 515.58, and 315.18 mg/g, respectively, at pH 7.11 and 25 °C. The results showed that AOFI had a very high adsorption capacity. These values were higher than those obtained by hydroxyapatite nanoparticles (HAP) for Cr(III), Pb(II) and Cu(II) (96.9, 440.5 and 69.9 mg/g, respectively) [51]. The adsorption capacities of AOFI were also lower than those of N-functionalized mesoporous silicas (SBA-15) for Cr(III), Pb(II), and Cu(II) (57.7, 185.6, and 111.2 mg/g, respectively) [52]. However, AOFI had higher adsorption capacities than polyethylene, polypropylene, and polyethylene terephthalate microplastic particles for Cr(III), Pb(II), and Cu(II), which ranged from 0.2 to 2.9 mg/g [53]. The LODs of AOFI for Cr(III), Pb(II), Cu(II), and iodine were 20.91, 22.01, 19.28, and 44.00 ppm, respectively, which were lower than those obtained by the energy dispersive X-ray fluorescence spectrometry [54]. These values were much higher than those obtained by other adsorbents, such as polymethylmethacrylate-organobentonite nanocomposite [55], dithizone grafted poly(allyl chloride) core–shell–shell magnetic nanoparticles [56], and chitosan-reduced graphene oxide hydrogel [57]. Therefore, AOFI was a promising adsorbent for the removal and detection of Cr(III), Pb(II), Cu(II), and iodine from aqueous solutions.

6 Conclusion

The primary objective of this study was to assess the efficacy of activated *Opuntia ficus-indica* (AOFI) as an adsorbent for the heavy metals and iodine uptake. Collected from Al-Baha city, KSA, AOFI underwent carbonization and thorough characterization using FT-IR spectroscopy, TGA and XRD analysis. Uptake experiments were systematically conducted, encompassing Cr(III), Pb(II), Cu(II) ions, and iodine at various initial concentrations, contact times, and pH values. Adsorption capacities for iodine, Cr(III), Pb(II), and Cu(II) were diligently determined for both AOFI and its precursor, OFI. The outcomes revealed noteworthy differences between the two materials. AOFI exhibited a significantly enhanced adsorption capacity compared to OFI, showcasing respective increments of 1.14, 1.14, and 1.16 times for Cr(III), Pb(II), and Cu(II). Additionally, AOFI demonstrated a 1.05 times higher adsorption capacity than OFI for iodine uptake. These results underscore the superior adsorption performance of AOFI over its precursor OFI across a range of heavy metal ions and iodine. The

Langmuir isotherm model aptly described the adsorption process, indicating monolayer adsorption on homogeneous sites. Moreover, the pseudo-second-order kinetics model suggested a chemisorption mechanism. The optimal pH for efficient metal and iodine removal was identified at approximately 6–7. Impressively, AOFI exhibited excellent reusability, retaining over 80% of their initial adsorption capacity after five regeneration cycles. Results further revealed that AOFI exhibited remarkable efficiency in the uptake of metal ions, achieving removal efficiencies of up to 70%, while demonstrating notable efficiency in iodine removal, reaching up to 60%. These findings underscore the exceptional uptake capabilities of AOFI for both metal ions and iodine, positioning it as a promising adsorbent for water treatment applications. In conclusion, this study not only addressed the specific objectives related to heavy metal and iodine uptake but also contributed novel insights, innovative concepts, and improvements compared to existing literature. Moving forward, future work should explore the full potential of AOFI in diverse water treatment scenarios and continue to refine our understanding of its unique adsorption properties.

Acknowledgements The author acknowledges Al-Baha University in providing the facilities for the present work.

Funding The authors declare that no funds, grants, or other support were received during the preparation of this manuscript.

Data availability All data generated or analyzed during this study are included in this published article.

Declarations

Conflict of interest There are no conflicts to declare.

Open Access This article is licensed under a Creative Commons Attribution 4.0 International License, which permits use, sharing, adaptation, distribution and reproduction in any medium or format, as long as you give appropriate credit to the original author(s) and the source, provide a link to the Creative Commons licence, and indicate if changes were made. The images or other third party material in this article are included in the article's Creative Commons licence, unless indicated otherwise in a credit line to the material. If material is not included in the article's Creative Commons licence and your intended use is not permitted by statutory regulation or exceeds the permitted use, you will need to obtain permission directly from the copyright holder. To view a copy of this licence, visit http://creativecommons.org/licenses/by/4.0/.

References

1. Barbera M, Indelicato S, Bongiorno D, Censi V, Saiano F, Piazzese D (2023) Untreated *Opuntia ficus indica* for the efficient adsorption of Ni(II), Pb(II), Cu(II) and Cd(II) ions from water. Molecules 28(9):3953
2. Madhav S, Ahamad A, Singh AK, Kushawaha J, Chauhan JS, Sharma S, Singh P (2020) Water pollutants: sources and impact on the environment and human health. In: Pooja D, Kumar P, Singh P, Patil S (eds) Sensors in water pollutants monitoring: role of material. Springer Singapore, Singapore, pp 43–62
3. Chowdhary P, Bharagava RN, Mishra S, Khan N (2020) Role of industries in water scarcity and its adverse effects on environment and human health. In: Shukla V, Kumar N (eds) Environmental concerns and sustainable development: Air, Water and Energy Resources. Springer Singapore, Singapore, vol 1, pp 235–256
4. Mahi O, Khaldi K, Belardja M, Belmokhtar A, Benyoucef A (2021) Development of a new hybrid adsorbent from *Opuntia ficus indica* NaOH-activated with PANI-reinforced and its potential use in Orange-G dye removal. J Inorg Organomet Polym Mater 31:2095–2104
5. Choudhary M, Kumar R, Neogi S (2020) Activated biochar derived from *Opuntia ficus-indica* for the efficient adsorption of malachite green dye, Cu^{2+} and Ni^{2+} from water. J Hazard Mater 392:122441
6. Hadjittofi L, Prodromou M, Pashalidis I (2014) Activated biochar derived from cactus fibres—preparation, characterization and application on Cu(II) removal from aqueous solutions. Bioresour Technol 159:460–464
7. Crini G, Lichtfouse E, Wilson LD, Morin-Crini N (2019) Conventional and non-conventional adsorbents for wastewater treatment. Environ Chem Lett 17:195–213
8. Crini G (2006) Non-conventional low-cost adsorbents for dye removal: a review. Biores Technol 97(9):1061–1085
9. Wawrzkiewicz M, Bartczak P, Jesionowski T (2017) Enhanced removal of hazardous dye form aqueous solutions and real textile wastewater using bifunctional chitin/lignin biosorbent. Int J Biol Macromol 99:754–764
10. Shoukat R, Cappai M, Pia G, Pilia L (2023) An updated review: *Opuntia ficus indica* (OFI) chemistry and its diverse applications. Appl Sci 13(13):7724
11 Lim T (2011) *Opuntia ficus-indica*, edible medicinal and non-medicinal plants: Volume 1, fruits. Springer, Berlin, pp 660–682
12. Al-Sulbi AO (2008) Ecological impact prediction of coastal reclamation in the Dammam Metropolitan Area. The University of Manchester, Manchester
13. Nharingo T, Moyo M (2016) Application of *Opuntia ficus-indica* in bioremediation of wastewaters. A critical review. J Environ Manag 166:55–72
14 Martins M, Ribeiro MH, Almeida CM (2023) Physicochemical, nutritional, and medicinal properties of *Opuntia ficus-indica* (L.) Mill. and its main agro-industrial use: a review. Plants 12(7):1512
15 Barbera M, Gurnari G (2018) Wastewater treatment and reuse in the food industry. Springer, Berlin
16 Alqurashi AS, Al Masoudi LM, Hamdi H, Abu Zaid A (2022) Chemical composition and antioxidant, antiviral, antifungal, antibacterial and anticancer potentials of *Opuntia ficus-indica* seed oil. Molecules 27(17):5453
17. Nasrollahzadeh M, Sajjadi M, Maham M, Sajadi SM, Barzinjy AA (2018) Biosynthesis of the palladium/sodium borosilicate nanocomposite using *Euphorbia milii* extract and evaluation of its catalytic activity in the reduction of chromium(VI), nitro compounds and organic dyes. Mater Res Bull 102:24–35
18. Barzinjy AA, Hamad SM, Aydın S, Ahmed MH, Hussain FH (2020) Green and eco-friendly synthesis of Nickel oxide nanoparticles and its photocatalytic activity for methyl orange degradation. J Mater Sci Mater Electron 31:11303–11316
19. Jabbar KQ, Barzinjy AA, Hamad SM (2022) Iron oxide nanoparticles: preparation methods, functions, adsorption and coagulation/flocculation in wastewater treatment. Environ Nanotechnol Monit Manag 17:100661
20. Sajadi SM, Kolo K, Hamad SM, Mahmud SA, Barzinjy AA, Hussein SM (2018) Green synthesis of the Ag/bentonite

nanocomposite using *Euphorbia larica* extract: a reusable catalyst for efficient reduction of nitro compounds and organic dyes. ChemistrySelect 3(43):12274–12280
21 Azeeza HH, Barzinjya AA (2020) Biosynthesis zinc oxide nanoparticles using *Apium graveolens* L. leaf extract and its use in removing the organic pollutants in water. Desalin. Water Treat 190:179–192
22. Guedes BN, Fathi F, Silva AM, Santini A, Oliveira MBP, Souto EB (2023) Biopharmaceutical applications of *Opuntia ficus-indica*: bibliometric map, bioactivities and extraction techniques. Eur Food Res Technol 249(10):2457–2469
23. Torres-Acosta AA (2007) *Opuntia-ficus-indica* (Nopal) mucilage as a steel corrosion inhibitor in alkaline media. J Appl Electrochem 37:835–841
24. Araceli Mandujano R, Luis-Enrique Corona A, Héctor Herrera H, Jorge Morales H (2018) Opuntia ficus-indica (Nopal Extract) as green inhibitor for corrosion protection in industrial steels. In: Mahmood A (ed) Corrosion inhibitors, principles and recent applications. IntechOpen, Rijeka, p Ch. 7
25. Osuna HTG, Mendoza AB, Morales CR, Rubio EM, Star JV, Ruvalcaba RM (2014) Iodine application increased ascorbic acid content and modified the vascular tissue in *Opuntia ficus-indica* L. Pak J Bot 46(1):127–134
26. Kolya H, Kang C-W (2023) Bio-based polymeric flocculants and adsorbents for wastewater treatment. Sustainability 15(12):9844
27. Lee J-Y, Lee S-E, Lee D-W (2022) Current status and future prospects of biological routes to bio-based products using raw materials, wastes, and residues as renewable resources. Crit Rev Environ Sci Technol 52(14):2453–2509
28. Ummartyotin S, Pechyen C (2016) Strategies for development and implementation of bio-based materials as effective renewable resources of energy: a comprehensive review on adsorbent technology. Renew Sustain Energy Rev 62:654–664
29. Kassem MA, Walters SA, Groninger JW, Midden KS, Meksem K (2023) Proceedings of the fifth international American Moroccan agricultural, health, and life sciences conference (AMAHLS V Conference) and The First Cannabis & Hemp Sciences and Entrepreneurship Day (CHSE I), December 13–14, 2022, Tangier, Morocco. Atlas J Biol 768–829
30. Volpe M, Goldfarb JL, Fiori L (2018) Hydrothermal carbonization of *Opuntia ficus-indica* cladodes: role of process parameters on hydrochar properties. Biores Technol 247:310–318
31. Ali I, Hasan MA, Alharbi OM (2020) Toxic metal ions contamination in the groundwater, Kingdom of Saudi Arabia. J Taibah Univ Sci 14(1):1571–1579
32 Gil MAV, Casal D, Pevida C, Pis J, Rubiera F (2010) Thermal behaviour and kinetics of coal/biomass blends during co-combustion. Bioresour Technol 101(14):5601–5608
33. Petrović M, Šoštarić T, Stojanović M, Milojković J, Mihajlović M, Stanojević M, Stanković S (2016) Removal of Pb^{2+} ions by raw corn silk (*Zea mays* L.) as a novel biosorbent. J Taiwan Inst Chem Eng 58:407–416
34. Qasem NA, Mohammed RH, Lawal DU (2021) Removal of heavy metal ions from wastewater: a comprehensive and critical review. Npj Clean Water 4(1):36
35. Yu B, Zhang Y, Shukla A, Shukla SS, Dorris KL (2000) The removal of heavy metal from aqueous solutions by sawdust adsorption—removal of copper. J Hazard Mater 80(1–3):33–42
36. Bozbaş SK, Boz Y (2016) Low-cost biosorbent: Anadara inaequivalvis shells for removal of Pb(II) and Cu(II) from aqueous solution. Process Saf Environ Prot 103:144–152
37. Saeed A, Akhter MW, Iqbal M (2005) Removal and recovery of heavy metals from aqueous solution using papaya wood as a new biosorbent. Sep Purif Technol 45(1):25–31
38. Li Q, Lu H, Xiao H, Gao K, Diao M (2013) Adsorption capacity of superabsorbent resin composite enhanced by non-thermal plasma and its adsorption kinetics and isotherms to lead ion in water. J Environ Chem Eng 1(4):996–1003
39. Robati D (2013) Pseudo-second-order kinetic equations for modeling adsorption systems for removal of lead ions using multi-walled carbon nanotube. J Nanostruct Chem 3:1–6
40. Mathai CJ, Saravanan S, Anantharaman M, Venkitachalam S, Jayalekshmi S (2002) Effect of iodine doping on the bandgap of plasma polymerized aniline thin films. J Phys D Appl Phys 35(17):2206
41. Yang Y, Xiong X, Fan Y, Lai Z, Xu Z, Luo F (2019) Insight into volatile iodine uptake properties of covalent organic frameworks with different conjugated structures. J Solid State Chem 279:120979
42. Abdelmoaty YH, Tessema T-D, Choudhury FA, El-Kadri OM, El-Kaderi HM (2018) Nitrogen-rich porous polymers for carbon dioxide and iodine sequestration for environmental remediation. ACS Appl Mater Interfaces 10(18):16049–16058
43. Sabri MA, Al-Sayah MH, Sen S, Ibrahim TH, El-Kadri OM (2020) Fluorescent aminal linked porous organic polymer for reversible iodine capture and sensing. Sci Rep 10(1):15943
44. Aravindhan R, Fathima NN, Rao JR, Nair BU (2007) Equilibrium and thermodynamic studies on the removal of basic black dye using calcium alginate beads. Colloids Surf A 299(1–3):232–238
45. Li W, Wang J, He G, Yu L, Noor N, Sun Y, Zhou X, Hu J, Parkin IP (2017) Enhanced adsorption capacity of ultralong hydrogen titanate nanobelts for antibiotics. J Mater Chem A 5(9):4352–4358
46. Taşar Ş, Kaya F, Özer A (2014) Biosorption of lead(II) ions from aqueous solution by peanut shells: equilibrium, thermodynamic and kinetic studies. J Environ Chem Eng 2(2):1018–1026
47. Langmuir I (1918) The adsorption of gases on plane surfaces of glass, mica and platinum. J Am Chem Soc 40(9):1361–1403
48. Sivaraj R, Namasivayam C, Kadirvelu K (2001) Orange peel as an adsorbent in the removal of acid violet 17 (acid dye) from aqueous solutions. Waste Manag 21(1):105–110
49. Freundlich H, Hatfield H (1926) Colloid and capillary chemistry. Methuen and Co, Ltd., London, pp 110–114
50. Treybal RE (1980) Mass transfer operations. N Y 466:493–497
51. Si Y, Huo J, Hengbo Y, Wang A (2018) Adsorption kinetics, isotherms, and thermodynamics of Cr(III), Pb(II), and Cu(II) on porous hydroxyapatite nanoparticles. J Nanosci Nanotechnol 18(5):3484–3491
52. Kobylinska N, Dudarko O, Kessler V, Seisenbaeva G (2021) Enhanced removal of Cr(III), Mn(II), Cd(II), Pb(II) and Cu(II) from aqueous solution by N-functionalized ordered silica. Chem Afr 4(2):451–461
53. Han X, Wang S, Yu X, Vogt RD, Feng J, Zhai L, Ma W, Zhu L, Lu X (2021) Kinetics and size effects on adsorption of Cu(II), Cr(III), and Pb(II) onto polyethylene, polypropylene, and polyethylene terephthalate microplastic particles. Front Mar Sci 8:785146
54. Tho P, Van H, Nguyen L, Hoang T, Tran N, Nguyen T, Nguyen T, Nguyen V, Sy H, Thai V (2021) Enhanced simultaneous adsorption of As(III), Cd(II), Pb(II) and Cr(VI) ions from aqueous solution using cassava root husk-derived biochar loaded with ZnO nanoparticles. RSC Adv 11:18881–18897
55. Abu-Zurayk RA, Hamadneh I, Al-Taee, BJ, Al-Kayed MF, Al-Dujaili AH (2023) Adsorption of Pb(II) and Cr(III) ions and p-chlorophenol on polymethylmethacrylate-organobentonite Nanocomposite. Polymer Bulletin
56. Zhang L, Gao X, Xiong Z, Zhang L, Yu B, Zhang R, Zhang W (2015) Preparation of dithizone grafted poly(allyl chloride) core–shell–shell magnetic composite microspheres for

solid-phase extraction of ultra-trace levels of Pb(II), Cu(II) and Cr(III) ions. RSC Adv 5(72):58873–58879

57. Tho P, Van HT, Nguyen LH, Hoang TK, Tran TNH, Nguyen TT, Nguyen TBH, Le Sy H, Tran QB, Sadeghzadeh SM (2021) Enhanced simultaneous adsorption of As(III), Cd(II), Pb(II) and Cr(VI) ions from aqueous solution using cassava root husk-derived biochar loaded with ZnO nanoparticles. RSC Adv 11(31):18881–18897

Publisher's Note Springer Nature remains neutral with regard to jurisdictional claims in published maps and institutional affiliations.